

Spatial variations of the effective elastic thickness, T_e , using multitaper spectral estimation and wavelet methods: examples from synthetic data and application to South America

M. Pérez-Gussinyé

Institute of Earth Sciences “Jaume Almera” (CSIC), Barcelona, Spain

Now at: Department of Earth Sciences, Royal Holloway University, London, UK

C. J. Swain and J.F. Kirby

Dept. of Spatial Sciences, Curtin University of Technology, Perth, Australia

A. R. Lowry

Department of Geology, Utah State University, Logan, Utah, USA

Abstract

Improved recovery of the spatial variability in the effective elastic thickness, T_e , of the lithosphere is important to interpret Earth's structure and geodynamics. Here we use synthetic topography and gravity data to systematically compare the recovery of T_e using the multitaper windowing scheme of Pérez-Gussinyé et al. (2004, 2007) with the wavelet approach of Kirby and Swain (2008a). We find that spuriously high T_e estimates previously present in synthetic tests with the multitaper are artefacts arising from Fourier transform edge effects introduced by splitting the data into land and ocean areas prior to load deconvolution. Hence, we adopt the mixed land-ocean loading scheme of Kirby and Swain (2008). Using this approach we find that underestimation of T_e when the transitional wavelength approaches the window size is largely related to the limited size of the analysis window, and not to random correlations of initial loading surfaces as occurs in the wavelet method. To attenuate this bias we apply a correction factor to our resulting multitapered T_e and find that this technique more accurately recovers steep T_e gradients and small-scale T_e anomalies than the wavelet method. Finally, we recalculate T_e of South America using the multitaper and the mixed land-ocean approach. The new T_e distribution is very similar to that of Pérez-Gussinyé et al. (2007, 2008), suggesting that Fourier transform edge effects are less severe in the real Earth than in synthetic data. This difference arises because coastlines are much less rough in the real Earth than in our synthetic data. Based on the synthetic results, we interpret that most of the small-scale features present in multitaper but not in wavelet T_e estimates of South America (Tassara et al., 2007) are real. These include high T_e over the Andean flat subduction zones and low T_e along the dyke swarms of the Paraná flood basalts, the Tacutu graben and Amazonian basin.

1. Introduction

Improved methods to image geophysical observables and their lateral variations are key to understanding Earth's structure and geodynamics. One such observable is the effective elastic thickness, T_e , of the lithosphere, which is a proxy for its flexural rigidity and mainly reflects composition and temperature gradients within the lithosphere (*Burov and Diament, 1995; Lowry and Smith, 1995, Watts, 2001*). As such, maps of T_e can image the terranes that form the continents and the sutures that record their amalgamation (e.g. *Pérez-Gussinyé and Watts, 2005*).

Inverse methods to recover T_e compare the coherence function between the topography and Bouguer anomaly data against the predictions of a thin elastic plate model (*Forsyth, 1985*). To recover the spatial variations in T_e , most implementations of Forsyth's coherence method divide

the analysis area into overlapping windows of a given size where the coherence is computed and inverted in each window via load deconvolution. Since the coherence is a measure of the normalized cross-power spectrum of the topography and gravity data, T_e inversion relies on the optimum estimation of the spectra of windowed data, which requires tapering (see review in *Prieto et al.*, 2007), or on wavelet approximations of the spectra. Different tapering techniques yield different spectra, resulting in varying T_e values (*Audet and Mareschal*, 2004; *Ojeda and Whitman*, 2002). One of the most modern spectrum estimation techniques is the multitaper, which has been widely used to estimate T_e in different continents (*Simons et al.*, 2000; *Swain and Kirby*, 2003; *Audet and Mareschal*, 2004; *Pérez-Gussinyé and Watts*, 2005; *Pérez-Gussinyé et al.*, 2007; 2008). A shortcoming of any windowing technique, including the multitaper, is that the window size limits the wavelength information of the analyzed data. An attempt to overcome this problem consists of calculating the coherence using wavelet transforms (*Kirby and Swain*, 2004; *Swain and Kirby*, 2006; *Stark et al.*, 2003). In the wavelet method, the signal is convolved at each point of the data grid with a family of wavelets that have a range of scales. Small-scale wavelets reveal the short wavelength information, while large-scale wavelets reveal the longest-wavelength information of the data.

The results from multitaper windowing and wavelet methods differ in their lateral resolution and the maximum T_e values recovered. The purpose of this work is to compare T_e recovery of both methods and assess T_e maps previously obtained for South America. While the multitaper T_e estimates obtained by *Pérez-Gussinyé et al.* (2007, 2008) were not able to retrieve spatial variations within high T_e regions, those of *Tassara et al.* (2007) using the “fan” wavelets of *Swain and Kirby* (2006) were relatively smooth and did not resolve many of the shorter wavelength T_e features present in the multitaper studies. Such “short” wavelength features included high T_e over the Andean flat slab regions, which *Pérez-Gussinyé et al.* (2008) interpreted as thick cratonic lithosphere. This and other considerations led those authors to relate the occurrence of flat subduction with the presence of rigid, cratonic lithosphere near the trench. Ultimately, understanding which features in T_e maps are real is important to discriminate tectonic models deriving from T_e estimates.

To comprehensively compare the methods, we use the same synthetic topography and Bouguer anomaly data generated by *Kirby and Swain* (2008a) for the analysis of their “fan” wavelet method (described in *Swain and Kirby*, (2006)). These authors found that the wavelet method underestimated T_e by 10% due to random correlations of the initial loads. Additionally, they established that the wavelet method tends to smooth out large lateral T_e gradients.

In previous work, *Pérez-Gussinyé et al.* (2004, 2007) had tested the ability of the multitaper method to recover T_e using different window sizes. They found that when the transition wavelength at which the coherence is 0.5 is large relative to the window size, most of the resulting T_e values were underestimated and additionally that the number of spuriously high T_e estimates, or outliers, increased. They concluded that when T_e is constant, larger windows produce more accurate estimates. For spatially variable T_e they found a trade-off between spatial resolution, which improves with smaller windows, and the recovery of large T_e values, which improves with larger windows.

Here we revise the multitaper method used in *Pérez-Gussinyé et al.* (2004, 2007, and 2008) after comparing it with the wavelet results presented by *Kirby and Swain* (2008a). We find that the outliers present in previous tests with synthetic data are artefacts due to the separate load deconvolution of masked land and ocean data. Hence, we adopt the *Kirby and Swain* (2008a)

deconvolution scheme for mixed land and ocean data and test the recovery abilities of our “new” method. We first describe our synthetic results with uniform and spatially variable T_e data sets and compare them to those obtained by Kirby and Swain (2008a). Subsequently, we show the updated T_e distribution for South America and assess the T_e structures resolved by the multitaper and wavelet methods.

3. Results of Synthetic Models

The synthetic data consist of grids of 256x256 points with spacing of 20 km, generated with fractal dimension of 2.5, subsurface loading at the 35 km deep Moho, and expected loading ratio, f , of 1. Kirby and Swain (2008a) give a detailed description of the data synthesis procedure and the values for crustal thickness, density of water, crust and mantle. Here we use multitaper parameters of $NW = 3$ and $K = 3$, where N is the number of samples within the data window, W is width of the main lobe of the first order taper and K is number of tapers (see Simons et al., 2001). The window size used for analysis is 600x600 km (as in Pérez-Gussinyé et al., 2008). When estimating T_e we deconvolve the wavenumber-dependent loading at the surface and sub-surface and evaluate the coherence fit assuming that loads are uncorrelated (Forsyth, 1985). We refer the reader to Pérez-Gussinyé et al. (2004, 2007) for a detailed description of the multitaper technique applied to T_e estimation and to Swain and Kirby (2006) for a description of their wavelet method. In the following we present the results of tests with the multitaper method.

3.1. Uniform T_e

3.1.1 Land/Ocean Loading

A number of authors have performed tests on synthetic data using a multitaper technique and found that for a given uniform T_e , the recovery degrades as the window size decreases (Swain and Kirby 2003; Audet and Mareschal, 2004; Crosby, 2007; Pérez-Gussinyé et al., 2004; 2007). While all of these studies found that T_e was generally underestimated, Pérez-Gussinyé et al. (2004, 2007) also found that some unconstrained high T_e estimates, which they called outliers, occurred. After observing that the incidence of outliers increased with decreasing window size, they interpreted these to result from insufficient sampling of the transitional wavelengths (see Figure 4 of Pérez-Gussinyé et al., 2007). However, careful comparison with estimates of Swain and Kirby (2003) hinted that the outliers were not just related to windowing. Systematic examination showed that they were artefacts caused by the separation of the data in land and ocean areas prior to load deconvolution. This procedure was used by Pérez-Gussinyé et al. (2004, 2007, 2008) and Lowry et al. (1994, 1995) to accommodate the variable surface fluid density of offshore and onshore data. It consisted of generating two pairs of topography and gravity anomaly grids, one pair in which data from the offshore regions were masked and one pair masked over land. Load contributions were deconvolved via equations (A1)–(A3) of Pérez-Gussinyé et al. (2004) using water densities for oceanic only data and air densities for land only data. After deconvolution the amplitudes were recombined to estimate the predicted coherence. Kirby and Swain (2008a) suggested this approach yields spectral leakage across discontinuities at the coastlines due to Fourier transform edge effects, which resulted in outliers as shown in Figure 1a. When the data are not split into land and ocean areas but ocean loading is instead approximated using an equivalent topography correction (Stark et al., 2003), the edge effects and outliers disappear (Figure 1b).

Fortunately, the incidence of outliers due to Fourier transform edge effects is much greater in synthetic data than in real data, as will be demonstrated by comparing new results for South America with those in Pérez-Gussinyé et al. (2008). This is because real-Earth coastal erosion

processes act to efficiently reduce the fractal dimension of coastline length, and hence the ratio of continental area to coastal length, relative to a random distribution of synthetically generated topography. We have used a random number generator to generate synthetic topography with a power law relationship of amplitude to wavenumber that mimics the spectral power of real topography (Turcotte, 1997). Because the algorithms used here to generate synthetic topography neglect the smoothing effect of ocean wave dynamics on coastline distributions (Sapoval *et al.*, 2004), zero crossings in the synthetic topography are much more ubiquitous than in the real Earth, resulting in spectral leakage effects across a broader range of wavenumbers than occurs in real data.

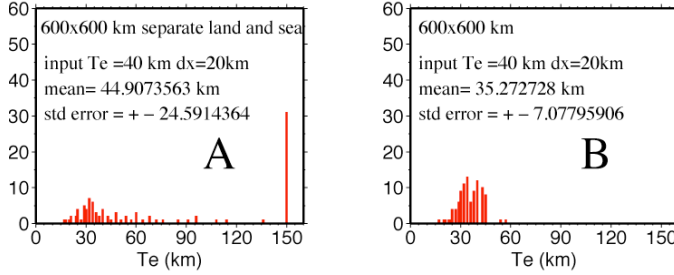


Figure 1. T_e recovery tests performed with 100 pairs of synthetic topography and Bouguer anomaly data generated with a spatially constant T_e of 40 km. Grid spacing is 20 km, multitaper parameters are $NW=3$, $K=3$, and the analysis window size is 600x600 km. For each topography and gravity anomaly data set the initial surface and subsurface load distributions is different. In **A** the estimates

after separating the data in land and ocean areas prior to load deconvolution are shown. This procedure generates edge effects in the Fourier Transform which result in outliers (here shown as T_e values of 150 km, see also Section 4.1. Mean and standard deviations shown here neglect the outliers). When ocean data are instead accommodated using the equivalent topography method, the outliers disappear and the standard deviation is much smaller, see **B**. From here on, all tests presented use the equivalent topography approach (see Section 4.1).

In all of the results that follow, we adopt the approach of Stark *et al.* (2003) and Kirby and Swain (2008a) to treat mixed land and marine environments. This approach scales ocean bathymetry, h , to an equivalent topography $h' = (\rho_c - \rho_w)h / \rho_c$ prior to Fourier transformation and application of the land loading equations to the entire data set. Kirby and Swain (2008) showed that, although this approach may bias T_e in ocean areas, the bias is small. The equivalent topography represents the bathymetry that would be expected if there were no water present (provided isostasy is local). This allows the loading equations for a land environment to be used.

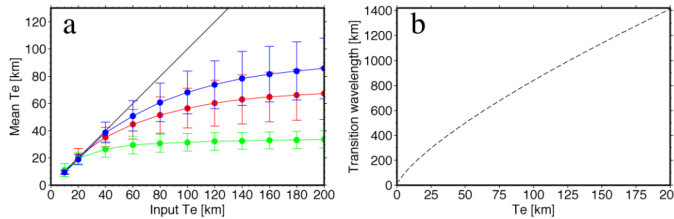


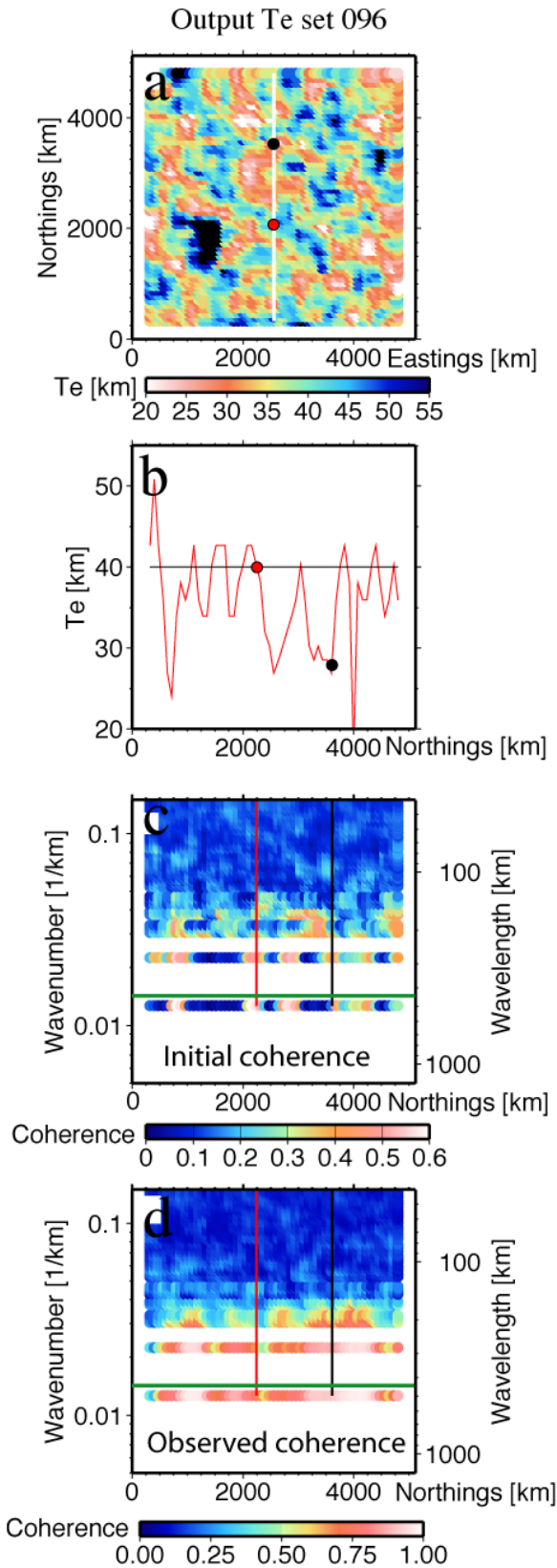
Figure 2. Mean T_e estimate and standard deviation versus input T_e , from tests with 100 synthetic topography and Bouguer anomaly data sets generated using spatially constant input T_e values of 10, 20, 40, 60, 80, 100, 120, 140, 160, 160 and 200 km. The standard deviations increase with input T_e of the

synthetic, as the transition wavelength for those T_e values increases relative to the window aperture used for analysis. We fit a regression curve (blue curve) to the data to define a correction for the downward bias resulting from the limited window size (see Section 4.2).

3.1.2 Downward Bias of T_e by Initial Load Correlation and Correction

Figure 2a shows the mean T_e and its standard deviation using 100 synthetic topography and gravity data sets, each with a spatially uniform T_e . The three colors indicate the results of the calculation using windows of different sizes of 400x400 km, 600x600 km and 800x800 km. Figure 2b shows the coherence transition wavelength, i.e. the transition at which the coherence is

1/2, for different T_e values. The coherence



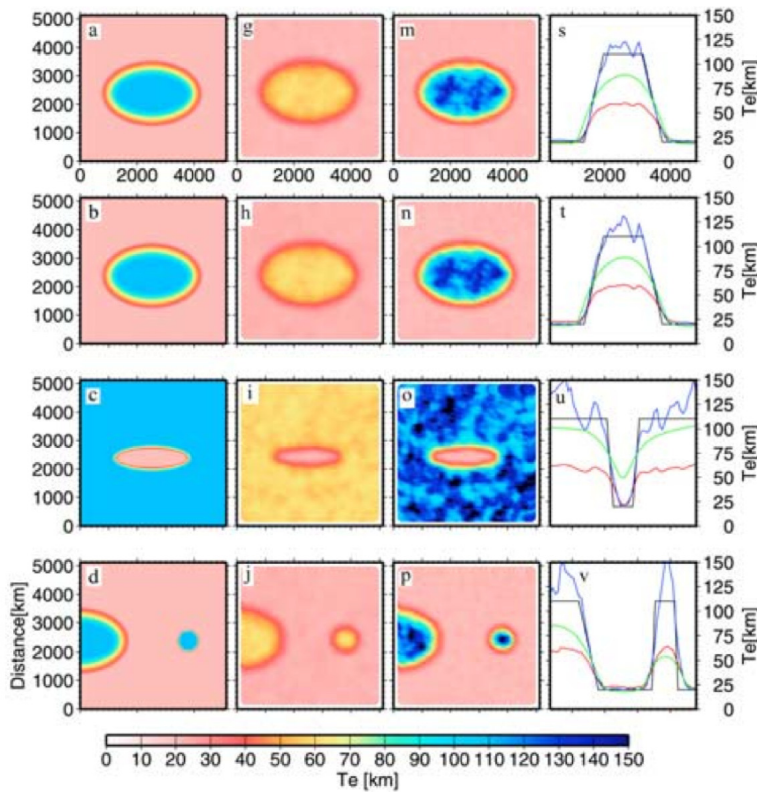
transition wavelength has been calculated using analytical expressions for the coherence for a given T_e and loading ratio (derived in the Appendix of Kirby and Swain, 2008a). The loading ratio used here is 1, the same that was used for synthetic data generation. The figure shows that recovery of T_e quickly degrades when the transitional wavelength approaches the window size. For conciseness, we focus in this work on window sizes of 600x600km. For this window recovery deteriorates significantly for input $T_e > 50$ km.

Figure 3. Analysis of correlation between surface and sub-surface loads. (a) T_e estimates from synthetic topography and gravity data sets 096 generated with an input T_e of 40 km. The white line shows the location of the T_e profile in (b). Red and black circles show reference locations discussed in the text (see Section 4.2). (c) shows the coherence between the initial surface and sub-surface loads along the white line shown in a. The red and black lines mark the value of the coherence at the locations given by the red and black circles in a and b. The green line marks the transition wavelength for a $T_e = 40$ km using the quartic equation of Kirby and Swain (2008b). (d) shows the coherence between the topography and gravity anomaly for the data sets 096. The green line marks the same as in c. The figure shows that locations where the T_e value is underestimated (e.g., at the red circle) do not necessarily coincide with locations where the initial surface and subsurface loads are correlated, as was suggested for the wavelet method of Kirby and Swain (2008a).

Forsyth's (1985) method is based on the assumption that surface and subsurface loads responsible for topography and gravity signals are statistically uncorrelated. Macario *et al.* (1985) used synthetic data to show that correlation between these loads would lead to underestimation of T_e . Subsequently, Kirby and Swain (2008) found that even if these loads are generated in such a way that they are truly uncorrelated, some degree of random correlation between initial surface and subsurface loads might occur at some locations after subsampling the data within wavelets. They demonstrated that when the wavenumbers of correlation between initial loads

coincided with the transitional wavelength of the input T_e , the coherence roll-over was biased towards shorter wavelengths, resulting in a 10% underestimation of T_e .

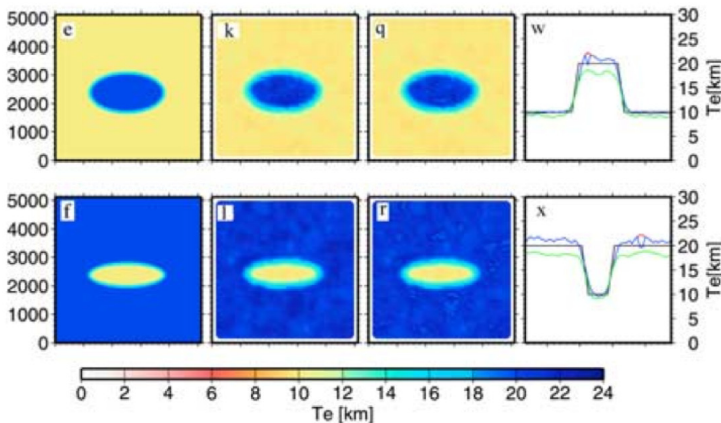
Figure 3 shows that when the multitaper method is used, initial load correlations do not clearly map into coherence roll-overs at shorter wavelengths. Figure 3a depicts the recovered T_e from synthetic topography and gravity data sets generated using a uniform T_e of 40 km. Figure 3b shows T_e values along the $x = 2560$ km profile. We focus on the coherence between initial loads (Figures 3c) and between final gravity and topography (Figure 3d) along this profile. At the black and red circles T_e is respectively underestimated and well estimated. Although the observed coherence roll-over is shifted towards shorter wavelengths where T_e is underestimated (Figures 3d), this is not reflected in an increased coherence between initial loading surfaces at this location (Figures 3c). Hence, for the multitaper method, bias due to windowing is much greater than effects of initial load correlation. We hypothesize instead that this bias is due to low



signal-to-noise ratio at the longest wavelengths of tapered data, and lack of representation of longer wavelengths needed to recover higher T_e , favors lowered T_e estimates. Thus, the bias and standard deviation depends primarily on the ratio of the estimation window size to the flexural wavelength (as shown in Figure 2).

Figure 4. (a-f) Input T_e models, (i-n) mean recovered T_e , (o-t) mean recovered T_e after correction for downward bias with regression curve shown in Figure 2, (u-z) North south cross sections at $x=2560$ km of the input T_e (black), mean T_e (red) and mean T_e after correction (blue). The green line shows the T_e values recovered with the wavelet method along the same cross-section by Kirby and Swain (2008). a, c, d, e and f are data generated with land loading only, b is generated with land and ocean loading for comparison with a.

Therefore, we propose that T_e underestimation is mostly due to tapering and windowing. To correct for this bias, we adjust a regression line to the mean T_e . This is constructed by interpolating the mean T_e values shown in Figure 2 using a spline function. These



values are shown also in Table 1 so that the reader can perform the interpolation. Henceforward we use this regression curve to obtain more accurate recovery of synthetic as well as real T_e .

3.2. Spatially Variable T_e

3.2.1 Elliptical T_e Structures

Figure 4 shows the recovery using different elliptical T_e structures. In Figures 4a, c, d, e and f, the data have been generated assuming only land environments and in Figure 4b with land and ocean environments. In the latter, the mixed land-ocean approach of *Kirby and Swain* (2008a) is used. Comparison of Figure 4b and 4a shows that the corrected topography approach in land-ocean environments yields equally accurate T_e recovery as for land data only.

One major difference from *Kirby and Swain's* (2008a) wavelet results is that, when the input T_e is high (Figure 4a, b, c and d), the resulting underestimation of T_e is larger with the multitaper method, as one would expect from the relatively small window size used here. However, after upward correction of the mean T_e (Figure 4o to 4r), the resulting structure better reproduces the steep gradients and lateral extent of the T_e anomalies than in *Kirby and Swain* (2008a). Still, because the regression line used for T_e correction increases very slowly for input T_e values $\sim > 60$ km, high variance in estimated T_e is amplified by the correction (Figures 4u, v, w, x).

Figures 4d, 4l, 4r and 4x show that, as occurs with the wavelet method, the ability of the multitaper method to recover steep T_e gradients decreases with decreasing size of the T_e anomaly. This effect is, however, less abrupt than using wavelets (compare with Figure 7 in *Kirby and Swain*, 2008a). Additionally, *Kirby and Swain* (2008a) showed with this synthetic case that their wavelet method requires mirroring to properly image high T_e anomalies at the edges of the data windows, which is not required for the multitaper method. Finally, the recovery for elliptical structures that have low T_e (Figures 4e and f) are similar qualitatively to those obtained by *Kirby and Swain* (2008a).

3.2.2 A Faulted Fractal T_e Structure

Kirby and Swain (2008a) proposed that the decreased ability of the wavelet method to recover steep T_e gradients with decreasing size of the T_e anomaly could be related to the diameter of the anomaly being much less than the transition wavelet width, or to the steepness of the T_e gradient which could invalidate the decoupling assumption. The decoupling assumption states that adjacent observed wavelet coherences are independent, whereas in fact they are not, which may lead to distortion of the recovered T_e (*Kirby and Swain*, 2008a).

To separate these two effects they generated a structure consisting of a fractal T_e distribution with a jump in T_e of 60 km and of 100 km width, splitting the area in half (Figure 5a). The idea of generating a faulted structure of such a large extent is to remove the effect of the diameter of the anomaly. The underlying fractal T_e structure is generated to test the recovery of short wavelength variations in T_e .

Figure 5b shows the average of 100 inversions using the multitaper method. As occurs in the wavelet method, the short wavelength variations in T_e are smoothed to a degree proportional to the T_e value. In the multitaper method this occurs because the transitional wavelengths are much better resolved when they are smaller than the window size, leading to better resolved T_e . In the wavelet method it occurs because the extent of the high T_e anomalies is smaller than the wavelet width required for recovering these high T_e values.

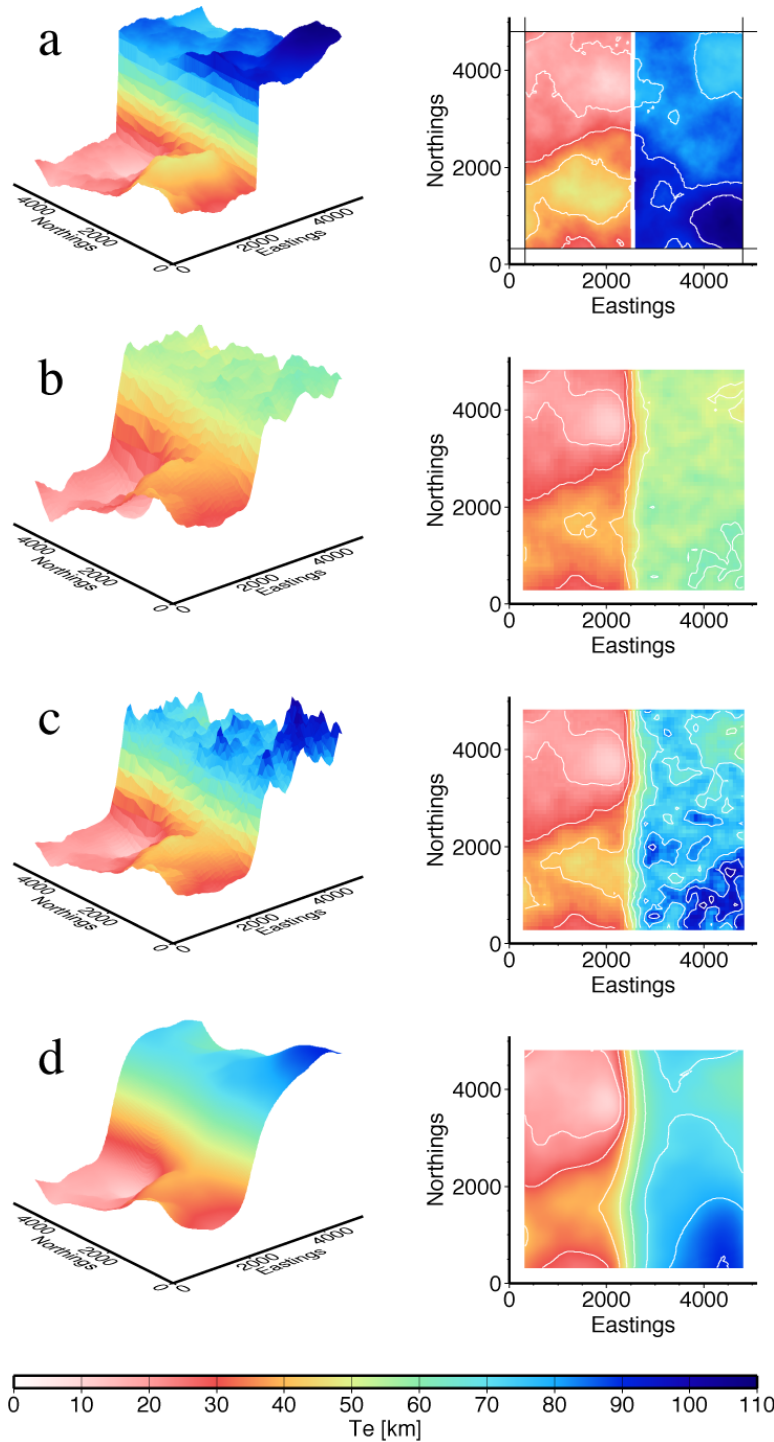


Figure 5. (a) Input T_e model, (b) mean T_e , (c) mean T_e after correction, (d) mean T_e recovered with the wavelet method by Kirby and Swain (2008). At left results are shown in perspective view and in plan view at right. White curves are contours at every 10 km T_e .

The recovery of the T_e variations greatly improves when the upward correction to T_e is applied (Figure 5c). Small-scale variations in the low T_e side of the structure, as well as the steep gradient, are much better resolved than in Figure 5b and also than using the wavelet method (Figure 5d). In the wavelet method, smoothing of the T_e gradient arises because the decoupling assumption is not fulfilled (Kirby and Swain, 2008a).

Although the upward T_e correction yields a much better recovery of the steep T_e gradient, it also introduces spurious short wavelength variations in the high T_e region of the structure. This arises because the correction curve amplifies already-high variance introduced by using a small window to recover large T_e values > 60 km. Hence, in the next section we apply this correction to real data but will assign no significance to lateral variations where $T_e > 100$ km.

4. Results with Real Topography and Gravity Data from South America

The results obtained after applying the mixed land-ocean deconvolution scheme with the multitaper method to South America are shown in Figure 6a. Figure 6b shows the resulting T_e corrected for the downward bias due to windowing. The image is very similar to that obtained in Pérez-Gussinyé *et al.* (2007, 2008), indicating that the effect of separating the data into land and ocean components prior to load deconvolution is not as severe as in synthetic data. As stated in Section 3.1.1, this is because real-Earth coastlines are less rough (and hence, land areas are more compact) than those of the synthetics.

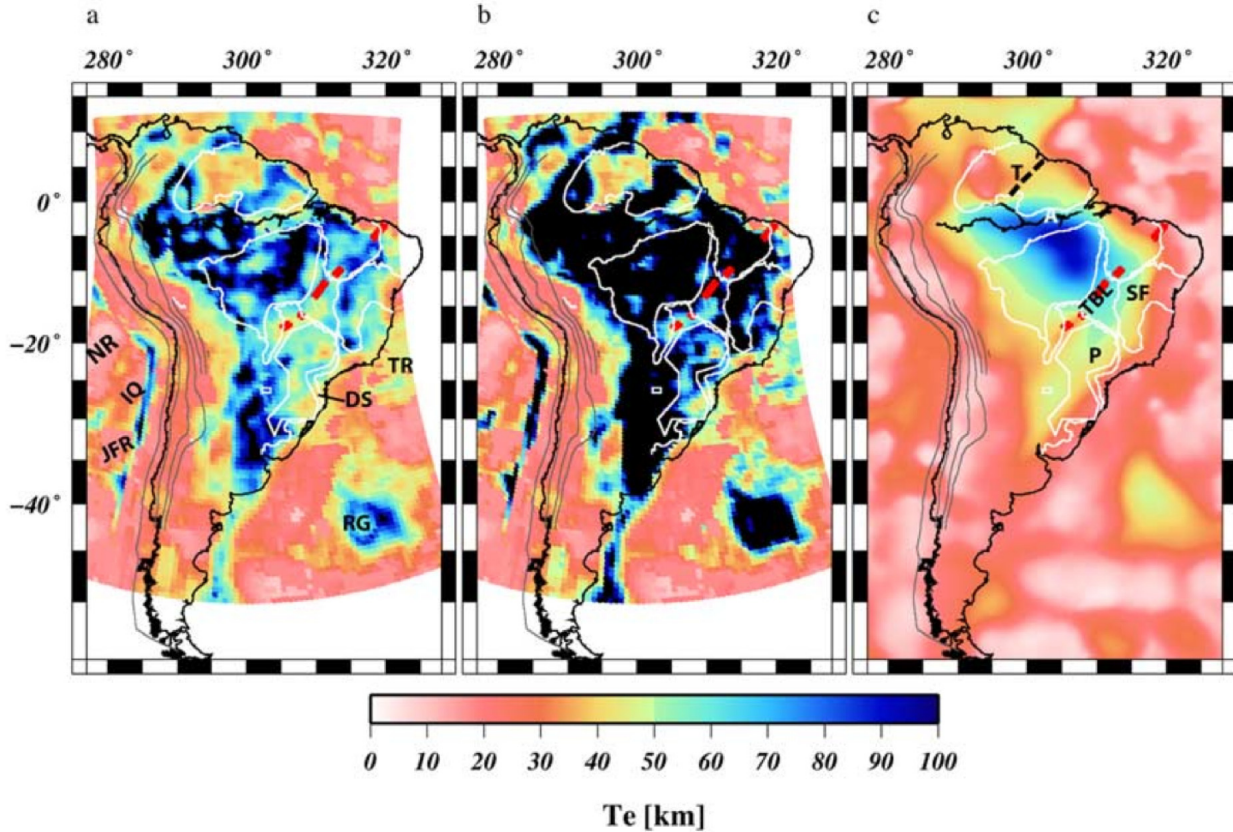


Figure 6. (a) T_e distribution for South America. Color scale goes only up to 100 km, as variations of T_e above this value are not well resolved. In black are T_e values larger than 100 km. (b) T_e distribution after correction for the downward bias due to the limited window size (c) T_e distribution using wavelets from *Tassara et al. (2007)*. In (a) NR, IQ and JF indicate the locations of the Nazca, Iquique and Juan Fernandez Ridges. DS indicates the locations of the dyke swarms that fed the Paran flood basalts, RG is the location of the Rio Grande Rise and TR marks the approximate location of the Trindade hotspot. In (c) P stands for Paran basin, SF for San Francisco Craton, TBL for Transbrasiliano suture, T for Tacutu graben and A for Amazonian basin. See *Prez-Gussiny et al. (2007)* for the gravity and topography data used in this analysis.

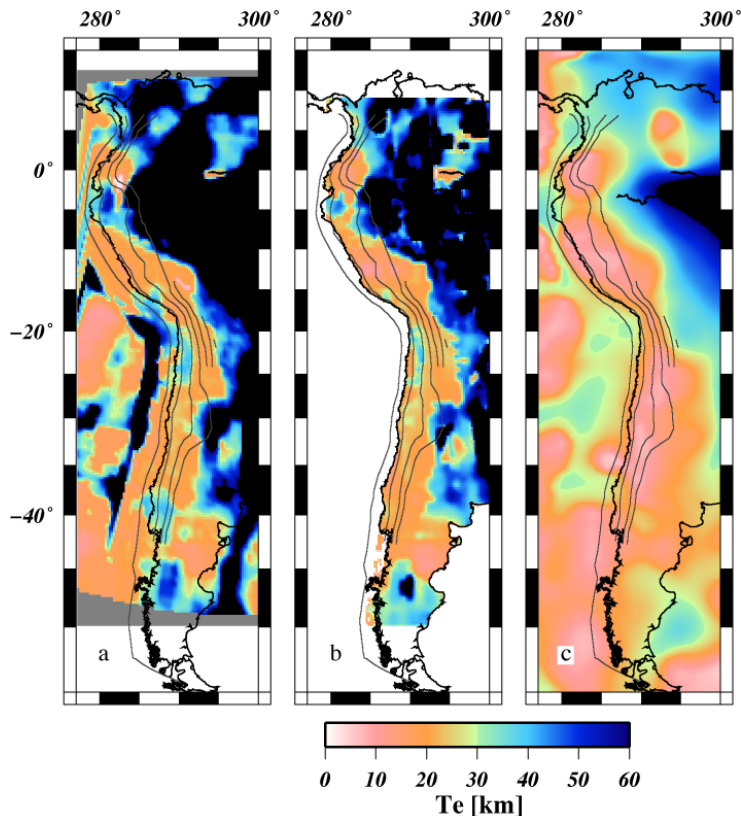
Our results show that old cratonic nuclei (mainly Archean and Early/Middle Proterozoic) have generally high T_e (>60 km), while the younger Phanerozoic terranes has much lower T_e (20–30 km). Although this implicit correlation of T_e to terrane age is consistent with other geophysical observations suggesting old cratonic nuclei to be thicker, colder, dryer and more depleted in basaltic constituents than lithosphere in younger provinces, some authors have suggested that T_e estimates > 30 km in cratonic interiors are incorrect (*Crosby, 2007; McKenzie, 2003*) because subsurface loads in highly eroded continental interiors lack topographic expression and hence reduce Bouguer coherence in a way that mimics an artificial increase in T_e . *Crosby (2007)* used synthetic topography and gravity anomaly data to show that if sub-surface loads with no topographic expression were modelled as noise in the gravity field, the Bouguer coherence would yield underestimates of T_e , and T_e estimates obtained using the free-air admittance would be more correct. However, *Prez-Gussiny and Watts (2005)* used both Bouguer coherence and free-air admittance over the ancient and highly eroded East European craton and obtained similarly high T_e estimates from each (> 60 km), indicating that if sub-surface loads with no topographic expression exist (in violation of the laws of continuum physics in a self-gravitating

body), they are not widespread and T_e is nevertheless high in cratonic areas.

Within the stable platform of South America, the low T_e areas imaged in this study encompass those described earlier by Pérez-Gussinyé *et al.* (2007). They coincide with part of the dyke swarms of the Paraná basin flood basalts, the Transbrasiliano suture, parts of the Amazonian rift and the Tacutu graben. Additionally, we image the fold belts separating the Paraná basin and San Francisco craton. Low shear wave seismic velocities at depth are also observed in this area using active seismic sources (Schimmel *et al.*, 2003).

For comparison we show the wavelet T_e results of Tassara *et al.* (2007) (Figure 6c). The differences between the latter and our T_e distribution are analogous to differences between our synthetic results and those of Kirby and Swain (2008a). The T_e gradients are less sharp using wavelets than multitaper, as observed for the fractal fault T_e synthetic (Figure 5). Also, some of the smaller scale low T_e features within high T_e cratonic South America, such as the Amazonian rift, parts of the Tacutu graben and the fold belts north of the Paraná basin, are not present in the wavelet results. We believe these structures have been smoothed in the wavelet results due to the high elastic thickness in the surrounding regions. In synthetic data, this occurs where a narrow ellipse of $T_e=20$ km is emplaced on a plate with T_e of 110 km (compare Figures 4k and 4q with Figure 4h of Kirby and Swain, 2008a).

Finally, the T_e estimates on the Andean side of South America are quite similar to those presented in Pérez-Gussinyé *et al.* (2008), with regions of high T_e in the Central Andes forearc and on top of the flat slab regions (Figure 7). They differ from those presented in Tassara *et al.* (2008), which do not clearly show these high T_e areas (Figure 7c). Since the synthetic data show that the wavelet method will spatially smooth small-scale high T_e areas within low T_e regions (see Figure 5b of Kirby and Swain, 2008a), we infer that all of these features present in the



multitaper results are real, and that they do not appear in Tassara *et al.*'s (2007) wavelet T_e because the large-scale wavelets employed in that study lack lateral resolution.

Figure 7. (a) Zoom of T_e distribution for the Andean part of South America using the corrected multitaper. (b) Zoom of the T_e distribution for the Andean part of South America using the multitaper version of Pérez-Gussinyé *et al.* (2008), in which separate load deconvolution for land and sea data were performed. As the figure shows, land estimates from real data are not affected as significantly by the load deconvolution method. (c) Zoom of the T_e distribution for the Andean part of South America using wavelets (from Tassara *et al.* (2007)). A color-scale that ranges up to T_e of 60 km is chosen for direct comparison with the results shown in Pérez-Gussinyé *et al.* (2008). In black are T_e values larger than 60 km.

5. Conclusions

We have revised the multitaper technique of *Pérez-Gussinyé et al.* (2004; 2007) and find that spuriously high T_e values observed in previous synthetic tests were artefacts resulting from Fourier transform leakage effects introduced by the separation of the data in land and sea regions for load deconvolution prior to T_e inversion. We have thus adopted the equivalent topography approach of *Kirby and Swain* (2008a) to treat mixed land-ocean environments.

Using this approach we find that T_e is systematically underestimated using the multitaper method due to limited size of the analysis window. This contrasts with the wavelet method where the underestimation mostly derives from random correlation of initial loading surfaces. To attenuate the downward bias we apply a correction factor to our multitaper estimates of T_e , resulting in a more accurate recovery of steep T_e gradients and small-scale T_e anomalies than with the wavelet method of *Kirby and Swain* (2008a).

Finally, we recalculate T_e of South America using the multitaper method and the mixed land-ocean approach. The new T_e distribution is very similar to that of *Pérez-Gussinyé et al.* (2007, 2008), suggesting that Fourier leakage effects at coastlines are less severe in the real Earth than in synthetic data. This difference arises because coastlines are much less rough, and land areas more compact, in real-Earth data than in synthetic data. In light of the synthetic results, we interpret that most of the small-scale features present in multitaper but not in wavelet T_e estimates of South America (*Tassara et al.*, 2007) are real. These include high T_e over the central Andean forearc and flat subduction zones and low T_e along the dyke swarms of the Paraná flood basalts, the Tacutu and Amazonian basins.

References

- Audet, P. and J.C. Mareschal (2004), Variations in elastic thickness in the Canadian Shield, *Earth and Planet. Sci. Lett.*, 226, 17-31.
- Burov, E., and M. Diament (1995), The effective elastic thickness (T_e) of the continental lithosphere: What does it really mean?, *J. Geophys. Res.*, 100, 3905-3927.
- Crosby, A., (2007), An assessment of the accuracy of admittance and coherence estimates using synthetic data, *Geophys. J. Int.*, 171, 25-54.
- Forsyth, D.W. (1985), Subsurface loading estimates of the flexural rigidity of continental lithosphere, *J. Geophys. Res.*, 90, 12,623-12,632.
- Kirby, J.F., Which wavelet best reproduces the Fourier power spectrum? (2005), *Computers and Geosciences*, 31, 846-864.
- Kirby, J.F. and C. J. Swain, (2004), Global and local isostatic coherence from the wavelet transform, *Geophys. Res. Lett.*, 31(24), L24608, doi:10.1029/2004GL021569.
- Kirby, J.F. and C. J. Swain, (2008a) An accuracy assessment of the fan wavelet method for elastic thickness estimation, *G-cubed*, 9, Q03022, doi:10.1029/2007GC001773.
- Kirby, J.F. and C. J. Swain, (2008b) An accuracy assessment of the fan wavelet method for elastic thickness estimation, *G-cubed*, 9(5), Q05021, doi:10.1029/2008GC002071.
- Lowry, A.R. and R.B. Smith, Strength and rheology of the western US Cordillera (1995), *J. Geophys. Res.*, 100, 17,947-17,963.
- Lowry, A.R. and R.B. Smith, Flexural rigidity of the Basin and Range–Colorado Plateau–Rocky Mountain transition from coherence analysis of gravity and topography (1994), *J. Geophys. Res.*, 99, 20,123-20,140.

- Macario, A., A. Malinverno, and W. F. Haxby (1995), On the robustness of elastic thickness estimates, and the strength of the continental lithosphere, *J. Geophys. Res.*, *100*, 15,163-15,172.
- Ojeda, G.Y., and D. Whitman, (2002), Effect of windowing on lithosphere elastic thickness estimates obtained via the coherence method: results from northern South America, *J. Geophys. Res.*, *10* (B11), 2275, doi:10.1029/2001JB000114.
- Pérez-Gussinyé, M., Lowry, A. R., Watts, A. B. and I. Velicogna (2004), On the recovery of the effective elastic thickness using spectral methods: examples from synthetic data and from the Fennoscandian Shield, *J. Geophys. Res.*, *109*, doi: 10.1029/2003JB002788.
- Pérez-Gussinyé, M. and A. B. Watts (2005), The long-term strength of Europe and its implications for plate forming processes, *Nature*, *436*, 381-384, doi: 10.1038/nature03854.
- Pérez-Gussinyé, M., Lowry, A. R., Watts, A. B. (2007), Effective elastic thickness of South America and its implications for intracontinental deformation, *G-cubed*, *8*, Q05009, doi:10.1029/2006GC001511.
- Pérez-Gussinyé, M., Lowry, A. R. J. Phipps Morgan, A. Tassara (2008), Effective Elastic thickness variations along the Andean margin and their relationship to subduction geometry, *G-cubed*, *9*, Q02003, doi:10.1029/2007GC001786.
- Prieto, G.A., Parker, R.L., Thomson, D.J., Vernon, F.L., Graham, R.L., (2007), Reducing the bias of multitaper spectrum estimates, *Geophys. J. Int.*, *171*, 1269-1281.
- Sapoval, B., A. Baldassarri, and A. Gabrielli, A self-stabilized fractality of seacoasts through damped erosion, *Phys. Rev. Lett.*, *93*(9), #098501, 2004.
- Schimmel, M., Assumpcao, M. and J. VandeCar (2003), Upper mantle seismic velocity structure beneath SE Brazil from P- and S-wave travel time inversions, *J. Geophys. Res.*, *108*, 2191, doi:10.1029/2001JB000187.
- Simons, F.J., M.T. Zuber and J. Korenaga (2000), Spatospectral localization of isostatic coherence anisotropy in Australia and its relation to seismic anisotropy: Implications for lithospheric deformation, *J. Geophys. Res.*, *105*, 19,163-19,184.
- Stark, C. P., J. Stewart and C. J. Ebinger, (2003), Wavelet transform mapping of the effective elastic thickness and plate loading: Validation using synthetic data and application to the study of the South African tectonics, *J. Geophys. Res.*, *108*(B12), 2558, doi:10.1029/2001JB000609.
- Swain, C. J. and J. F. Kirby (2003), The effect of ‘noise’ on estimates of effective elastic thickness of the continental lithosphere by the coherence method, *Geophys. Res. Lett.*, *30*, 1574 doi:10.1029/2003GL017070.
- Swain, C. J. and J. F. Kirby (2006), An effective elastic thickness map of Australia from wavelet transforms of gravity and topography using Forsyth’s method, *Geophys. Res. Lett.*, *23*, doi: 10.1029/2005GL025090.
- Tassara, A., Swain, C., Hackney, R. and J. Kirby, Elastic thickness structure of South America estimated using wavelets and satellite-derived gravity data (2007), *Earth and Planet. Sci. Lett.*, *253*, 17-36.
- Watts, A. B. (2001), *Isostasy and flexure of the lithosphere*, Cambridge University Press.